第32卷第10期 焊 接 学 报 Vol. 32 No. 10
2011年10月 TRANSACTIONS OF THE CHINA WELDING INSTITUTION October 2011

焊接顺序对T形接头残余应力和变形的影响

黎超文， 王 勇， 韩 涛
(中国石油大学 机电工程学院，东营 257061)

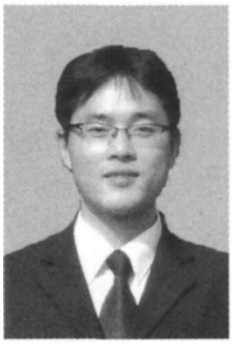

黎超文

摘 要：采用有限元热弹塑性分析方法对T形接头不同焊接顺序的残余应力和变形进行模拟. 有限元模型中选用三维实体单元，分析了材料物性参数随温度的变化和对流、辐射散热的影响. 运用单元生死技术模拟T形接头多道焊接过程，获得了不同焊接顺序T形接头焊接温度场和残余应力、变形场，并对计算结果进行了分析. 结果表明，焊接顺序对T形接头的残余应力和变形有较大的影响，采用先焊一侧，然后焊另一侧的方案所得到的残余应力和角变形最小.

关键词：T形接头； 有限元模拟； 焊接顺序； 残余应力； 焊接变形
中图分类号：TG404 **文献标识码**：A **文章编号**：0253－360X(2011)10－0037－04

0 序 言

随着计算机的飞速发展和大型有限元软件应用的日益成熟，采用科学的有限元数值模拟技术和少量的试验验证方法，实现对复杂焊接现象的模拟，获得焊接应力和变形的变化规律，能优化结构设计和工艺参数设计.

国内外的工作者对T形接头焊接结构的残余应力场和变形进行了一些研究，如张利国等人[1]从分段焊、多道焊、多段焊与多层焊的焊接顺序对简单T形接头焊接残余应力场的影响进行了研究. 薛小龙等人[2]研究了T形接头单面焊的应力和变形，但对T形接头双面焊接工艺优化方面的研究较少，尤其是对T形接头焊接顺序的工艺优化方面. 设计的非线性有限元软件从焊接顺序对简单T形接头焊接残余应力和变形的影响进行了研究，得到了不同焊接顺序下焊接残余应力和变形的分布，对T形接头焊接工艺方案的优化有重要的理论指导意义.

1 数学模型的建立

在区域Ω中三维瞬态温度场的控制方程为

$$\rho(T)\,C(T)\left(\frac{\partial T}{\partial t}\right)=\nabla\left(-\lambda(T)\cdot\nabla T\right)+Q^{\mathrm{TR}}(T,t) \tag{1}$$

式中：ρ 为材料的密度；C 为材料的热容；λ 为热导率；T 为温度；t 为时间；∇ 为哈密尔顿(Hamilton)算子；Q^{TR} 为内热源，包括弹塑性变形、蠕变和相变潜热等引起的变化；文中采用非线性分析，ρ，C，λ 均为温度的函数.

采用平衡方程和本构方程进行力学计算和分析，在区域Ω中力学平衡方程[3]为

$$\sigma_{ij,j}+\rho b_j=0 \tag{2}$$

式中：$\sigma_{ij,j}$ 为应力张量；b_j 为体积力.

应力应变本构方程为

$$[\mathrm{d}\boldsymbol{\sigma}]=[\boldsymbol{D}^{\mathrm{ep}}]\,[\mathrm{d}\boldsymbol{\varepsilon}]-[\boldsymbol{C}^{\mathrm{th}}]\,\mathrm{d}T \tag{3}$$

$$[\boldsymbol{D}^{\mathrm{ep}}]=[\boldsymbol{D}^{\mathrm{e}}]+[\boldsymbol{D}^{\mathrm{p}}] \tag{4}$$

式中：$[\boldsymbol{D}^{\mathrm{e}}]$ 为弹性刚度矩阵；$[\boldsymbol{D}^{\mathrm{p}}]$ 为塑性刚度矩阵；$[\boldsymbol{C}^{\mathrm{th}}]$ 为热刚度矩阵；$\mathrm{d}\boldsymbol{\sigma}$ 为应力增量；$\mathrm{d}\boldsymbol{\varepsilon}$ 为应变增量；$\mathrm{d}T$ 为温度增量.

2 物理模型的建立

采用焊条电弧焊，焊接工艺为：焊接电流110～130 A，电弧电压22～25 V，有效功率系数0.65，焊接速度2.5 mm/s. 为了研究双边焊缝焊接顺序对焊接残余应力和变形的影响，设计了4种方案，如图1所示，图中的箭头表示焊接方向，黑点表示焊接起始点，①与②表示焊接顺序.

3 数值模拟

3.1 计算模型

采用Visual-mesh软件建立的三维有限元模型

收稿日期：2010－09－13
基金项目：国家863高技术研究发展计划资助项目(2008AA09A106)

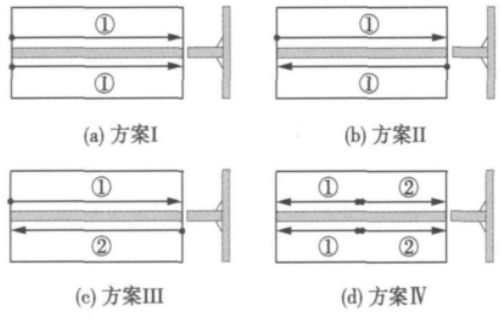

图1 4种焊接方案示意图

Fig. 1 Schematic diagram of four types of welding

和网格(图2),在焊接过程中,焊缝及其附近区域的温度场与应力场变化非常剧烈,因此,这些区域采取加密的网格,在远离焊缝的区域,能量传递缓慢,温度梯度变化较小,可采用相对稀疏的单元网格. 总之,在保证精度的同时尽量减少网格的数量.

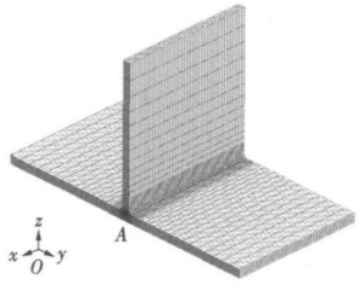

图2 有限元模型与网格

Fig. 2 Finite element model and mesh

3.2 焊接热源

为提高有限元计算的准确性,选择合适的热源模型是非常必要的. 文中采用了 Goldak 提出的双椭球热源模型[4],其热源分布函数为

$$q(x,y,z,t)=\frac{6\sqrt{3}f_{f,b}\eta UI}{abc_f\pi\sqrt{\pi}}e^{-3x^2/a^2}e^{-3[y+v(\tau-t)]^2/c_{f,b}^2}e^{-3z^2/b^2} \tag{5}$$

式中:f_f 和 f_b 分别为前后椭球能量分配系数,且 $f_f+f_b=2$; η 为热效率系数; τ 为焊接热源的滞后时间; U 和 I 分别为电弧电压、焊接电流; v 为焊接速度; a, b, c_f, c_b 为双椭球热源模型参数,各参数可由实际焊缝剖面的尺寸得到.

3.3 相变潜热

焊缝金属熔化和凝固时要吸收和放出热量,故需要考虑相变的影响. 假定熔化潜热等于凝固潜热并通过热容上升或者下降的变化来计算熔化潜热对焊件热焓值的影响. 取熔化潜热为 277 kJ/kg,固相线温度为 1 480 ℃,液相线温度为 1 520 ℃.

3.4 单元生死技术

有限元模型采用单元生死技术来模拟焊缝金属的逐步填充,在焊接开始之前,"杀死"所有的焊缝单元,使单元格的质量、热容和应变等设置为"零"状态,这些未被激活的单元格不参与分析计算. 随着电弧的移动,焊缝单元格逐步被激活,恢复到"生"的状态,其相关的质量、热容变为原始值,施加相应的荷载,并参与随后的分析计算.

3.5 时间和步长

将焊接过程分为电弧加热和冷却两个过程,采用自适应加载步长由焊接温度和时间共同控制,允许每步分析的最大温度变化为 150 ℃,允许每步分析的最小时间步长为 0.05 s. 为了兼顾计算效率和计算精度,划分温度区间并设置不同的收敛准则. 相变温度附近,收敛温度准则设置相对严格,使计算过程更好的考虑相变潜热的影响.

4 计算结果与分析

4.1 焊接顺序对热循环的影响

图3为距 A 点 35 mm 处一点($x=35$ mm, $y=0$)在4种焊接顺序下的热循环曲线.

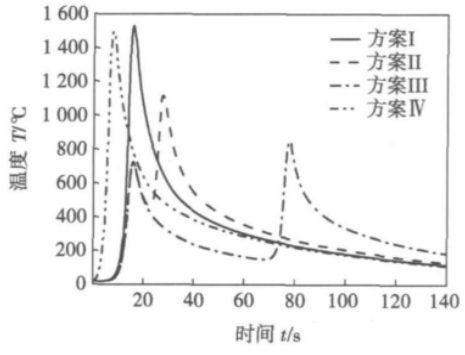

图3 焊接顺序对热循环的影响

Fig. 3 Effect of welding sequence on thermal cycle

焊接电弧不直接对该点进行加热,而是通过热传导使此点温度升高,由图3可知,4种焊接方案可分为两种类型,只经历单次热循环,峰值温度较高(方案Ⅰ和Ⅳ);经历两次热循环,峰值温度较第一种类型低(方案Ⅱ和Ⅲ). 这是由于第一种类型采用的是对称焊接,由于两个电弧同时对T形接头加热,焊接接头获得的热量较多,峰值温度高. 第二种类型的两个电弧依次对T形接头加热,第一个热循环对第二个热循环有预热作用,所以第二个热循环的峰值温度比第一个稍高. 方案Ⅱ中前道焊缝对后道焊缝的预热作用比较明显,而在方案Ⅲ中,前一

道焊缝的热量经过长时间的传导和周围介质的散失,在开始下一道焊缝时,焊件的温度非常低.

4.2　焊接顺序对残余应力的影响

由文献[1]可知,平行焊接方向的应力是最大的,其它方向的应力相对较小,且由于焊接过程中焊缝附近 ±20 mm 范围内的应力变化最为剧烈,研究了焊接顺序对该区域平行焊接方向的纵向残余应力(σ_x)的影响,如图 4 所示.

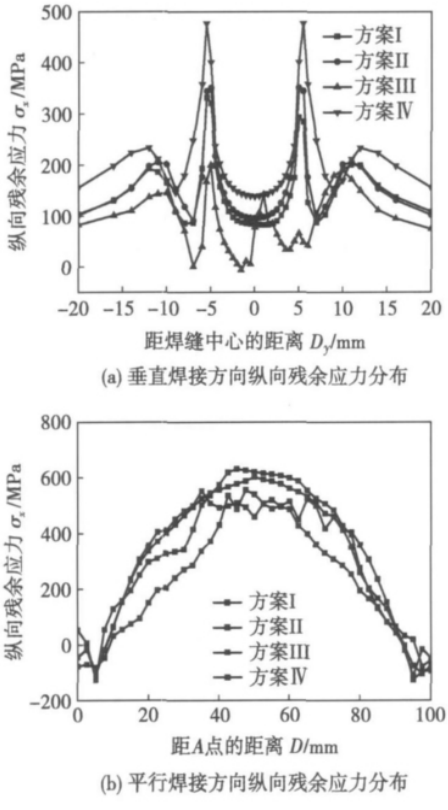

图 4　焊接顺序对残余应力的影响

Fig. 4　Effect of welding sequence on distributions of residual stress

图 4a,b 的分析路径分别为底板上表面垂直焊接方向距 A 点 35 mm(x = 35 mm)的直线和平行焊接方向距 A 点 6 mm(y = 6 mm)的直线. 从图 4a 中可以看出,焊缝以及焊缝附近存在残余拉应力,纵向残余应力的最大值应在两侧角焊缝的焊趾处. 由图 4b 可知,在焊缝起弧端和收弧端的焊趾存在残余压应力,但压应力的幅值相对较小,而在底板中部的焊趾逐渐转换为残余拉应力,且离底板边缘距离增加,残余拉应力幅值也增大. 局部区域的应力水平超过基体的屈服强度,这是导致构件容易发生开裂的主要原因.

由图 4 还可以看出,焊接顺序不仅影响残余应力的产生,而且对残余应力的分布和大小也有较大的影响. 拉应力最大值出现在第 4 种焊接方案,第 3 种焊接方案时的残余拉应力最小(图 4a),这主要是因为第二道焊缝对第一道焊缝有回火作用,这在一定程度上起到了消除应力的作用.

4.3　焊接顺序对变形的影响

从理论上来说,对于 T 形接头,焊接时在底板厚度方向(z 轴)上的温度分布是不均匀的,焊缝的一面受热发生膨胀,另一面膨胀小甚至不膨胀. 由于焊接面膨胀受阻,产生了较大的横向压缩塑性变形,在焊后冷却时就在焊缝厚度方向上出现收缩不均匀的现象,导致角变形的产生,如图 5 所示.

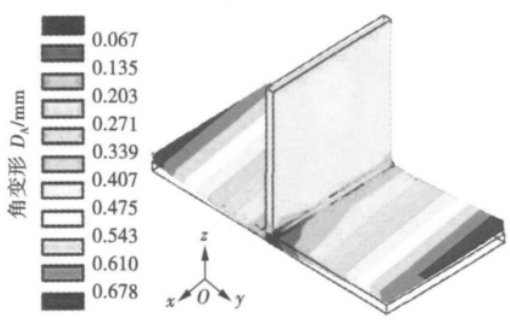

图 5　方案 II 时的角变形

Fig. 5　Angular distortion of case II

图 6 所示为焊接顺序对 T 形接头变形的影响. 由于约束了焊缝 z 轴方向的自由度,焊缝的变形非常小,随着离焊缝中心的距离增加,焊接变形逐渐增大,由图 6a 可知,4 种焊缝方案的角变形幅值由小到大的顺序依次为: 方案Ⅳ,Ⅱ,I 和 III,焊接变形主要是因为焊接电弧的热作用引起的[5],在方案 III 中,采用先焊一道焊缝,再焊另一道焊缝的方案,T 形接头的变形最小,其主要原因是 T 形接头获得的热量最少(图 3). 由图 6 还可以看出,焊缝两侧的焊接变形不同,第一道焊缝侧的变形较小(0.13 mm),第二道焊缝侧的变形相对上一道焊缝大(0.44 mm).

不同焊接顺序的 T 形接头纵向弯曲变形如图 6b 所示,4 种焊接方案的纵向弯曲变形值都较小; 方案 I 和方案 III 的纵向弯曲变形随着距离的变化而变化,方案 I 中,纵向弯曲变形沿着电弧运动方向的距离增加而增加,焊缝起弧位置变形较小,收弧位置的变形达到最大值(0.38 mm). 方案 III 中,纵向弯曲变形沿着第二道焊缝电弧运动方向的距离增加而略有增加. 方案Ⅱ和方案Ⅳ的纵向弯曲变形沿焊缝电弧运动方向基本没有变化.

由以上分析可知,T 形接头获得的热量是影响焊后变形的主要原因,由于方案 III 采用先焊一道焊

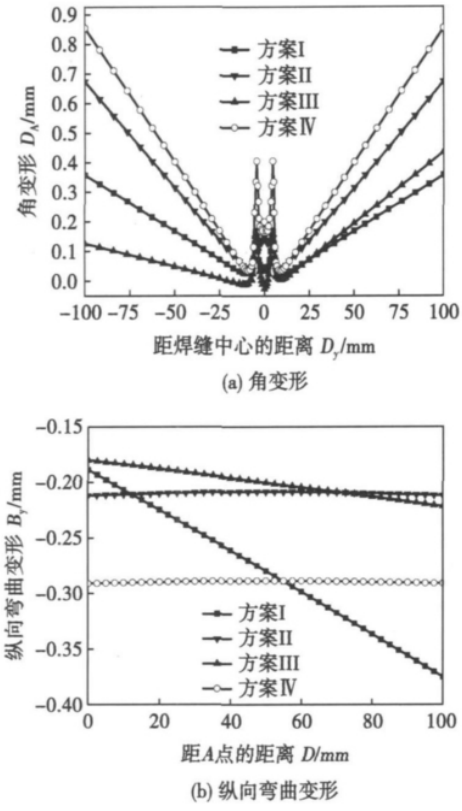

图6 焊接顺序对变形的影响

Fig. 6 Effect of welding sequence on distortion

缝,再进行另一道焊缝的方式,T形接头获得的热量最少,最终所获得的角变形最小,且由于后道焊缝对前一道焊缝的回火作用,焊缝接头的残余应力部分得到释放,最终接头的残余拉应力最小. 但是,由于T形接头两侧焊缝填充的不均匀性,所产生的残余拉应力、角变形和纵向弯曲变形也是不均匀的.

5 结 论

(1) 焊接顺序对T形接头的残余应力和变形有较大的影响,采用先焊一侧,然后焊另一侧的方案所得到的残余应力和角变形最小. 由于T形接头两侧焊缝填充的不均匀性,所产生的残余拉应力,角变形和纵向弯曲变形也是不均匀的.

(2) T形接头焊接时,焊缝以及附近区域获得的是残余拉应力,且最大值位于热影响区;在焊缝两端表现为残余压应力,但幅值较小,焊缝中部获得了较大的残余拉应力,局部区域的应力水平超过基体的屈服强度,这是导致构件更容易发生开裂的主要原因.

(3) 焊件受热不均是产生角变形的主要原因,获得的热量大小将决定角变形的大小. 纵向弯曲变形值较小.

参考文献:

[1] 张利国,姬书得,方洪渊,等. 焊接顺序对T形接头焊接残余应力场的影响[J]. 机械工程学报,2007,43(2):234-238.
Zhang Liguo, Ji Shude, Fang Hongyuan, *et al*. Influence of welding sequence on welding stress of T joing [J]. Chinese Journal of Mechanical Engineering, 2007, 43(2): 234-238.

[2] 薛小龙,王志亮,桑芝富,等. T形焊接接头的三维有限元模拟[J]. 中国机械工程,2005,16(9):811-815.
Xue Xiaolong, Wang Zhiliang, Sang Zhifu, *et al*. Three dimensional simulation of T-joing by SEM [J]. Chinese Mechanical Engineering, 2005, 16(9): 811-815.

[3] Sattari Far I, Farahani M R. Effect of the weld groove shape and pass number on residual stresses in butt-welded pipes [J]. International Journal of Pressure Vessels and Piping, 2009, 86(11): 723-731.

[4] Goldak J, Chakravarti A, Bibby M. A new finite element model for welding heat sources [J]. Metallurgical and Materials Transactions B, 1984, 15(2): 299-305.

[5] Kim Y C, Chang K H, Horikawa K. Production mechanism of out-of-plane deformation in fillet welding [J]. Transactions of the JWRI(Japan Welding Research Institute), 1998, 27(2): 107-113.

作者简介: 黎超文,男,1983年出生,博士研究生. 主要从事新材料连接技术和焊接结构完整性的研究. 发表论文20余篇. Email: lichaowen96@163.com

stress

Effect of welding sequences on welding residual stress and distortion of T-joint LI Chaowen, WANG Yong, HAN Tao (College of Mechanical and Electronic Engineering, China University of Petroleum, Dongying 257061, China). p 37 - 40

Abstract: This paper analyzes the thermo mechanical behavior and evaluates the welding residual stresses and distortion with various types of welding sequence in T-joint welds by performing thermal elasto-plastic analysis using finite element techniques. The 3-D solid elements are used in FE model, and material properties depending on the temperature are considered as well as the convection and radiation as boundary conditions. The stress distributions and distortion field are obtained. The welding residual stress and distortion are largely influenced by the welding sequences. When welding was performed continuously from one side to the other side, the magnitude of residual stress and distortion was the smallest.

Key words: T-joint; finite element simulation; welding sequence; residual stress; welding deformation

Influence of particle size on structure of HA/BG bioactive coatings ZHUANG Minghui, YIN Ke, LI Muqin, LI Xiaoxia (Provincial Key Laboratory of Biomaterials, Jiamusi University, Jiamusi 154007, China). p 41 - 44, 48

Abstract: HA/BG bioactive coatings were sprayed on Ti6Al4V substrate by subsonic flame spraying, and Ti/G coating was selected as transition player to relieve the stress in the coatings. HA/BG bioactive coatings underwent crystallization treatment at 700 ℃. The structure of the coatings was decided by the particle size. With fine particle, porous coatings can be obtained whose structure is beneficial to the bonding of the coatings and the bone tissue. After the crystallization treatment, the main phase of the HA/BG coatings was crystal HA, and the addition of fine active glass inhabited the growth of HA crystal. The compression stress exhibiting in HA/BG coatings was positive to improve the bonding strength of the coatings.

Key words: subsonic flame spraying; bioglass; transition player; particle size

AC arc stability of environmental protective type of basic and low hydrogen electrode MENG Gongge[1], CHU Jijun[2], LUAN Jingyue[2], GU Feng[1], LI Dan[1] (1. School of Material Science & Engineering, Harbin University of Science and Technology, Harbin 150040, China; 2. Harbin Welding Institute, China Academy of Machinery Science and Technology, Harbin 150080, China). p 45 - 48

Abstract: An electrode coating slag system CaO-CaF_2-BaO-TiO_2-SiO_2 has been designed base on analyzing several domestic and abroad basic slag systems. The experiments were done with uniform design method and computer aided analysis. Nine to eleven coating components were taken as independent variables and they were divided into five levels in all twenty nine experiments. The AC arc stability was taken as target function and data were analyzed with mathmatical statistic software. The results given the influencing trend figures of coating components on AC arc stability and multinomial mathematical model between independent variables and function. With these trend figures and mathematical model the improving direction of electrode for AC arc stability can be inquired and be searched target optimization.

Key words: basic electrode; AC arc stability; uniform design; optimization searching

TIG butt welding between Mg alloy and Al alloy filling with Zn wire LIU Fei, ZHANG Zhaodong, LIU Liming (Key Laboratory of Liaoning Advanced Welding and Joining Technology, School of Materials Science and Engineering, Dalian University of Technology, Dalian 116024, China). p 49 - 52

Abstract: Butt welding experiments of Mg to Al alloy filling with Zn wire were carried out by tungsten inert gas (TIG) welding. The welding joints were investigated and tested by metallography microscope, electronic probe micro-analyzer (EPMA), universal mechanical properties testing machine. The results indicated that the aluminum alloy 6061 and the magnesium alloy AZ31B was jointed with a good surface forming. The welded joints are mainly composed of $MgZn_2$, the zinc base solid solution and the aluminum base solid solution, there are not the obvious transitional layer between welded seam and aluminum base metal and the transitional layers which approximately 20 - 100 μm between welded seam and magnesium base metal. The hardness of the weld seam is higher than that of the base metal aluminium alloy 6061 and magnesium alloy AZ31B. The tensile strength of the butt joint is 75 MPa.

Key words: distributable metal of Mg and Al; butt welding filling with zinc wire; microstructures; mechanical properties; TIG

Strength and microstructure of Cu joints brazed with Cu-P based amorphous filler metal contained Zr GAO Fei, XU Weilong, WANG Chao, ZOU Jiasheng (Provincial Key Laboratory of Advanced Welding Technology, Jiangsu University of Science and Technology, Zhenjiang 212003, China). p 53 - 56

Abstract: The copper joints were brazed with CuP 7.7Sn5.4Ni14Si0.2Zr0.04 amorphous filler metal and conventional filler metal. The microstructures of filler metal and brazing joints were analyzed and the effect of brazing procedures on joints strength was studied. The results indicate that brazing procedures affect the strength of the brazing joints with both the CuP7.7Sn5.4Ni14Si0.2Zr0.04 amorphous filler metal and conventional filler metal. Compared to the amorphous brazing filler metal, conventional filler metal was more sensitive to the brazing procedure. In the same experimental conditions, shear strength of the joint brazed with amorphous brazing filler metal increased by 30% or more compared to the joint which brazed with conventional filler metal. CuP7.7Sn5.4Ni14Si0.2Zr0.04 amorphous brazing filler metal has no obvious phase structures in microscope, while the microstructure of conventional filler metal is mainly composed of primary $(Cu,Ni)_3P$ and $(\alpha$-$Cu + Cu_3P)$ eu-